SYNERGY
PUBLISHING PTE. LTD.

Volume 7
Issue 01
April 2023

ISSN 2591-7110(Print) 2591-7129(Online)

Modern Electronic Technology

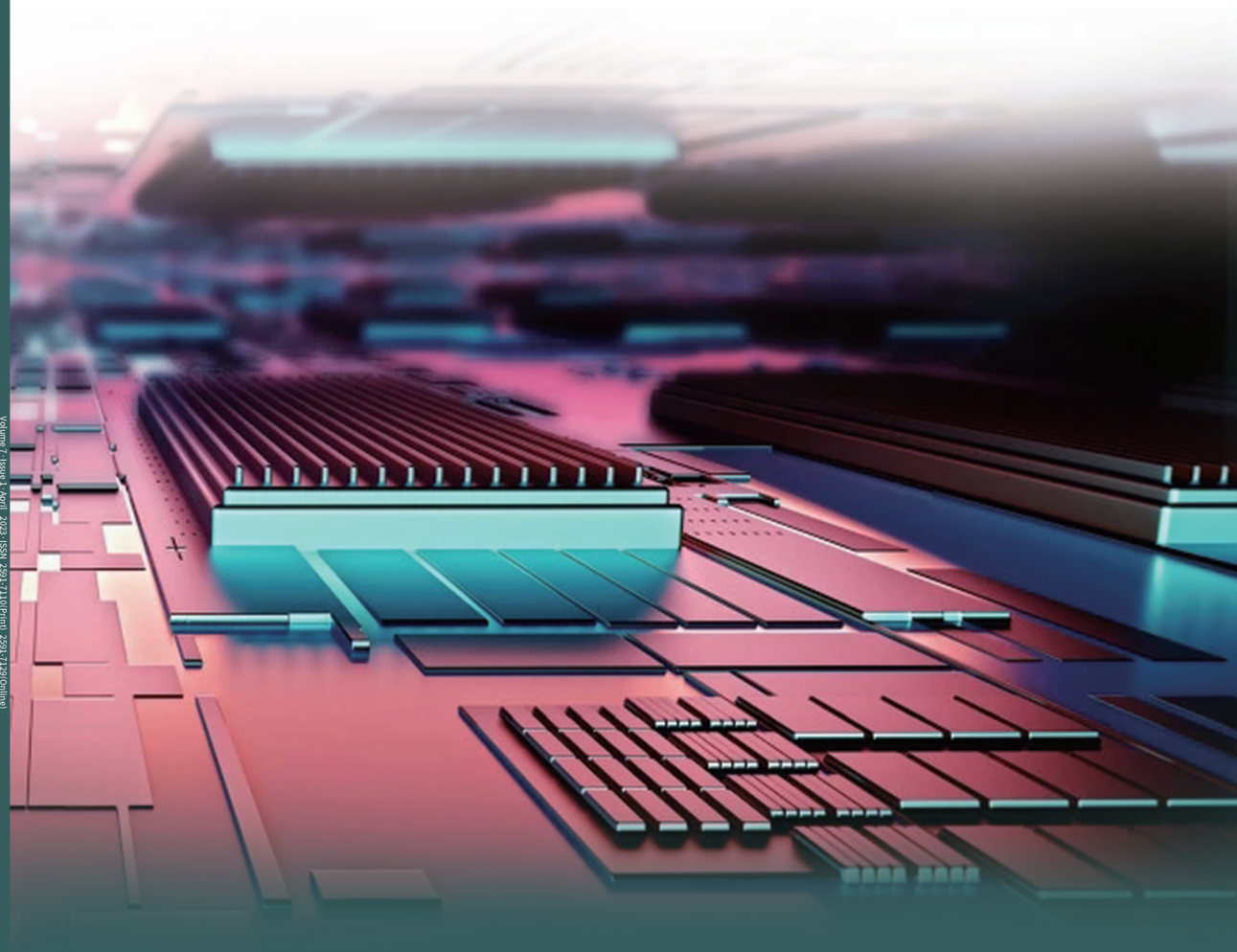

Modern Electronic Technology

Volume 7 Issue 1 April 2023 ISSN 2591-7110(Print) 2591-7129(Online)

SYNERGY
PUBLISHING PTE. LTD.
Tel: +65 65881289
E-mail: contact@s-p.sg
Website: ojs.s-p.sg

2591-7110 01
9 772591 711238

SYNERGY
PUBLISHING PTE. LTD.

Modern Electronic Technology

Aims and Scope

Modern Electronic Technology (MET) is an open access, peer-reviewed scholarly journal which aims to publish original research articles, reviews and short communications that covers all area of electronic engineering technology. MET emphasizes on publishing high quality papers, as well as aims to provide a source of information and discussion platform for engineers, researchers, and electronic professionals worldwide.

Subject areas suitable for publication include, but are not limited to the following fields:

- Microelectronics
- Nanoelectronics
- Electronic Materials Technology
- Structure and Nature of Semiconductor
- Digital Technology
- Automation System

Publishing Cycle

Quarterly

Journal Homepage

http://ojs.s-p.sg/index.php/met

Key Features

- Open Access
- High Academic Level Editorial Board
- Easy and Fast Submissions
- Double Blind Peer Review
- Rapid Online Publication of Articles upon Acceptance
- Outlet for Academic Institutions and Industry

SYNERGY PUBLISHING PTE. LTD.

Volume 7 Issue 1 · April 2023
ISSN 2591-7110 (Print) ISSN 2591-7129 (Online)

Synergy Publishing Pte.Ltd.

E-Mail: contact@s-p.sg
Official Website: www.s-p.sg
Address: 12 Eu Tong Sen Street, #07-169, Singapore 059819

CONTENTS

SYNERGY PUBLISHING PTE. LTD.

Modern Electronic Technology

http://www.advmodoncolres.sg/index.php/amor/index

Research of Strapdown Integrated Navigation System Based on Rotation Control Technology

Xu Dong[1] Jianshu Dong[1*] Hui Wang[2] Zongrui Yan[3]

1. Beijing Research institute of Mechanical & Electrical Technology, Beijing, 100074, China
2. Beijing Revitalization Institute of Measurement and Test, Beijing, 100074, China
3. Nanjing Naval Command Academy, Nanjing, Jiangsu, 210016, China

ARTICLE INFO

Article history
Received: 8 June 2022
Revised: 22 July 2022
Accepted: 15 September 2022
Published Online: 19 April 2023

Keywords:
Single-axial rotating
Control mechanism
PID
FOG
Inertial navigation

ABSTRACT

To realize high-precision Single-axial Rotating FOG-SINS, a low-power, low-cost, middle-precision rotating control mechanism design for single-axial rotating navigation system is put forward. Through theory analysis, design and experimental verification, the rotating control mechanism has good control precision and high reliability, which meets the demands for developing middle & high-precision FOG-SINS.

1. Introduction

Nowadays, foreign high-precision FOG-SINS is gradually replacing the expensive ESG inertial navigation system to provide ships with high-precision, low-cost and long-endurance inertial navigation system. In order to improve the accuracy of SINS based on the existing FOG, it is imperative to adopt the rotary modulation technology of error self-compensation.

At present, the continuous rotation alignment has become an effective technical means to achieve high-precision of FOG inertial navigation system. The technology of the continuous rotation scheme using single-axial rotating FOG-SINS is realized by the regular movement of the inertial measurement unit (IMU) of FOG around the rotation axis. By modulating the error of the inertial device in the rotation period, the drift error is compensated, and the growth of the error with time is controlled, so as to greatly improve the alignment accuracy and convergence speed of the system. Therefore, the technology has become one of the highlights of engineering application research.

2. Principle and Design Scheme

The single-axial rotating modulation technology of inertial navigation system is to install IMU on the single-axial rotation mechanism, which drives the IMU to rotate around the axis according to the set rule. The rotation axis

**Corresponding Author:*
Jianshu Dong,
Beijing Research institute of Mechanical & Electrical Technology, Beijing, 100074, China;
Email: treeplanter@163.com

 DOI: https://doi.org/10.26549/met.v7i1.11641

of the platform is perpendicular to the horizontal plane of the carrier. Under the normal reciprocating rotation control mode, the rotary mechanism drives the IMU to move from 0° to 360° of the optical code disk at a set rate, and then move from 360° to 0° for reciprocating rotation, based on the range value of the uniaxial angle measuring device [1,2].

Heading uncoupled reciprocating rotation mode is the superposition of heading tracking motion and reciprocating rotation motion. Assuming that the carrier is stationary, IMU will rotate according to the set rule. However, in practice, the carrier is always in various motions, and the angular motion of the carrier is coupled with the rotation of IMU. Under the influence of the carrier's heading motion, for the navigation system, IMU does not rotate according to the ideally set scheme, affecting the rotation modulation. In the navigation system, the equivalent gyro drift is related to the carrier's heading angle amplitude, angular frequency, the occurrence time of the carrier's heading, the time of heading angular motion and the rotation time of IMU relative to the carrier [3,4]. Due to the heading motion of the carrier, the motion of IMU in the navigation system is irregular. Within a rotation cycle, the error integral is not zero. That is, the course motion of the carrier offsets the modulation effect of IMU rotation. If the angle of the carrier's heading motion is always the same as the IMU's rotation angle relative to the carrier, and the direction is opposite, then the measurement error in the navigation system does not change, and the carrier's heading motion completely offsets the effect of rotation modulation. Ideally, using the calculated carrier's posture data and the set rotation modulation law to drive the IMU to rotate relative to the carrier can effectively eliminate the influence of the carrier's heading motion, and isolate the system from the carrier's heading motion, so that the IMU can rotate regularly relative to the navigation system. The positional relation between INS and IMU is shown in Figure 1 [5].

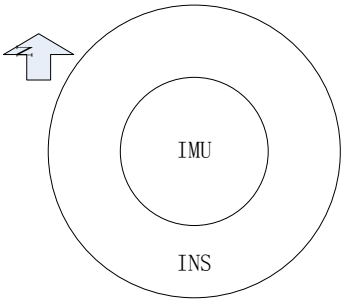

Figure 1. Positional relation between INS and IMU.

Heading uncoupled reciprocating rotation mode takes the geographical coordinate system as the benchmark and the demodulated initial heading angle as the zero position. According to the demodulated heading angle and angular velocity, it can reciprocate at a constant speed between 0° and 360°. The ideal situation is that no matter how the heading of the carrier (INS) changes, the rotating mechanism will rotate back and forth at a uniform speed around the reference angle of the geographic coordinate system [6-9].

The working principle of the rotating mechanism is as follows: The inertial measurement unit in the inertial navigation system is placed on the rotating mechanism, the DC motor drives the rotating mechanism to rotate through the gearbox and belt bearing, and the angular position is uploaded through the angle measuring device. The rotating mechanism returns to the zero position and waits for the command sent by the guidance computer. The rotating mechanism drives the inertial measurement unit to rotate at the set speed and rotation mode, or receives the position command sent by the guidance computer, turning to the required position at a fixed rate and stabilize at that position. At the same time, the real-time information of the rotating mechanism is transmitted to the external guidance computer through the serial port [10-12].

The rotation mechanism mainly realizes two functions: one is to receive the rate command sent by the guidance computer and rotate at the set rate and rotation mode; the second is to receive the position command sent by the guidance computer, turn to the required position at a fixed rate, and stabilize at this position. In addition, the rotating mechanism must also have the functions of power-on self-test and patrol inspection during operation, and send the results to the INS through the status word. If "stall" and other non hardware damage faults are found during the operation of the rotating mechanism, under the condition that the processor of the rotary control circuit can communicate with the inertial navigation system normally, the rotating mechanism shall be able to reset after the INS sends the reset command, and the control program shall be restarted [13-15].

The design scheme of the rotating mechanism considers the actual working requirements of the system, and integrates the sensor, processor and controller into a mechanical structure. The rotating mechanism is mainly composed of rotary control circuit, rotating control software, uniaxial angle measuring device, DC motor and other sub components. The composition and relationship of the rotating mechanism are shown in Figure 2. In the system, the rotary control circuit and its software collect the angle measurement information, realize the velocity driven by the motor, and communicate with the inertial navigation system. The guidance computer sends the same

DOI: https://doi.org/10.26549/met.v7i1.11641

synchronization signal to the rotary control circuit and the angle measuring device, and the rotary control circuit and the guidance computer simultaneously receive the angle measuring data sent by the angle measuring device. The small DC motor is responsible for the implementation of rotation function.

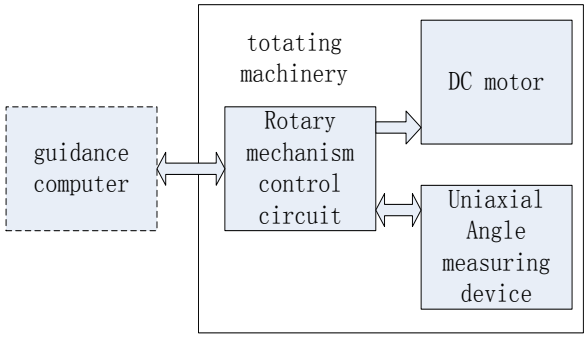

Figure 2. Rotary mechanism system.

3. Hardware Design

3.1 Design of Control Circuit

The rotary control circuit is responsible for collecting angle measurement information, driving the motor, communicating with the inertial navigation system, receiving instructions and sending data and status. The rotary control circuit obtains the accurate information of the angle measuring device at a fixed time. The control system drives the DC motor through the D/A converter and OP Amp, and uses it to form a complete motion control system with the processor, motor and angle measuring device. The 3D diagram of the rotary control circuit is shown in Figure 3.

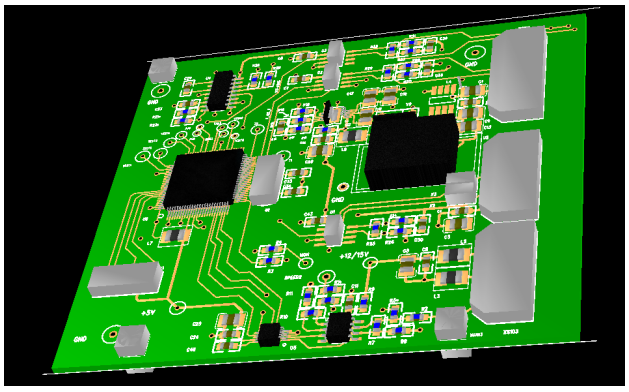

Figure 3. The 3D diagram of the rotary control circuit.

3.2 Selection of Uniaxial Angle Measuring Device

The uniaxial angle measuring device is mainly used in the angle measuring system of rotary mechanism. The rotary mechanism controls the movement of IMU according to the output angle signal of uniaxial angle measuring device, including angular position control and angular speed control. The rotary mechanism adopts the uniaxial angle measuring device of Changchun Institute of Optics, Fine Mechanicsand Physics, with a resolution better than 2.5”; response delay of synchronous signal shall not be greater than 5 μs; data output is less than 100 μs; power consumption is not greater than 1 W; the maximum allowable mechanical speed shall not be less than 20 rpm [16].

The working mode of the uniaxial angle measuring device is shown in Figure 4. The angle measuring device responds to the falling edge of the synchronization signal in an interrupt manner, triggers angle sampling, and then outputs angle data. From receiving the synchronization signal to completing the data output, it is less than 100 μs.

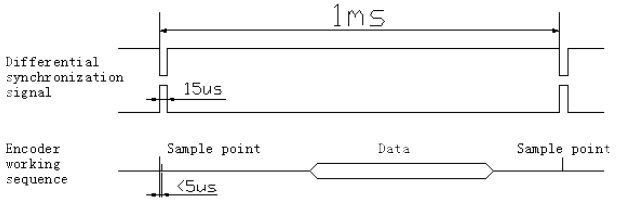

Figure 4. The working mode of the uniaxial angle measuring device.

The uniaxial angle measuring device sends the same synchronization signal to the rotary control circuit and the angle measuring device through the guidance computer, and the rotary control circuit and the guidance computer simultaneously receive the angle measuring data sent by the angle measuring device, as shown in Figure 5. The navigation software enters the 1 ms timing interrupt program. When the gyro is gated, the synchronization signal will be sent, and the maximum sampling delay after the angle measuring device receives the synchronization signal is 5 μs.

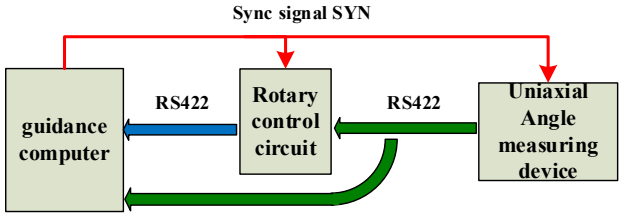

Figure 5. Diagram of data synchronization of rotary mechanism.

The conversion between digital quantity and arcsec of uniaxial angle measuring device is as follows:

$$1LSB = \frac{360^{(\circ)} \bullet 3600^{(")}}{2^{21}(=2097152)} \approx 0.618^{(")} \quad (1)$$

DOI: https://doi.org/10.26549/met.v7i1.11641

The digital quantity of uniaxial angle measuring device represented by 1 minute of arc is:

$$1^{(')} = \frac{2^{21}}{360^{(^\circ)} \bullet 60^{(')}} \approx 97.09 LSB \quad (2)$$

In the process of rotation, assuming that the angular velocity is 5, the angular error caused by the 5 ms software delay is:

$$\Delta\theta 1 = V_{速度} \bullet t_{时间} = \frac{5\,(^\circ/s) \bullet 3600^{('')}}{1^{(^\circ)} \bullet 1000S} \bullet 5ms = 90^{('')} \quad (3)$$

This formula indicates that the regulating accuracy is $90^{('')}$.

3.3 Selection of Motor

Measure and calculate the driving torque required by the 4.5 kg rotator, and the required torque is as follows:

3.3.1 Torque Required to Overcome Friction Torque

Friction torque includes the friction torque of uniaxial angle measuring device bearing, torque motor bearing and torque motor brush, the influence of lubricating grease on bearing friction torque, and the load increased by assembly error. The friction torque of the uniaxial angle measuring device is measured by hanging weights. The weight is 0.104 kg, and the arm of force is about 12.5 mm. The result is:

$$0.104 \times 9.8 \times 0.0125 = 0.01225\text{Nm} \quad (P = mgL) \quad (4)$$

The total friction torque of the motor, with a starting voltage of 0.6 V, is estimated as:

$$(0.7 \sim 0.8) \times 0.6/24 = (0.0175 \sim 0.02)\text{Nm} \quad (5)$$

Therefore, under normal temperature, the friction torque of the rotary mechanism is about 0.03 Nm. Considering the increase of friction torque at low temperature, the friction torque is taken as 0.1 Nm.

3.3.2 Torque Required for Acceleration of Rotary Mechanism

The maximum load generated by moment of inertia occurs at the end of commutation acceleration. At this time, according to the system requirements, the maximum angular speed of the rotary mechanism reaches 100 °/s (17 rpm), and the required torque is:

$$T_{j1} = J d\omega_1 /dt = 0.01969 \times 100/57.3 = 0.034\text{Nm} \quad (6)$$

3.3.3 Torque Required by Tracking Carrier Accelerative Rotation

According to the test data of a certain type of inertial navigation system, the instantaneous angular acceleration is not greater than 1500 °/s^2, so the torque to ensure the smooth rotation of the rotary mechanism is

$$T_{j2} = J d\omega_2/dt = 0.01969 \times 1500/57.3 = 0.515\text{Nm} \quad (7)$$

3.3.4 Torque Generated by Off-centre Rotating Part under Impact (15 g/11 ms)

According to the recalculation results, the eccentric distance of the rotating part is 0.23 mm, and the weight of the rotating body is 4.6 kg. Considering that the mechanism is amplified by 1.8 times, the actual acceleration reaches 27 g. Therefore, the torque generated by off-centre rotating part under impact is:

$$T_p = Mal = 4.6 \times 27 \times 9.8 \times 0.23 \times 10^{-3} = 0.28\text{Nm} \quad (8)$$

To sum up, the torque that the motor needs to provide under extreme conditions is the resultant force of the above torque, that is:

$$T = 0.1 + 0.034 + 0.515 + 0.28 = 0.929\text{Nm} \quad (9)$$

Considering that the probability of extreme conditions (e.g., carrier is 1500 °/s^2) is small, we balance the weight of the rotating body to reduce the eccentricity and 50% torque generated by shock, based on 50% of the extreme conditions, so the torque to be provided by the motor is:

$$T = 0.1 + 0.034 + 0.2575 + 0.15 = 0.54\text{Nm} \quad (10)$$

3.3.5 Calculation of Transmission between Uniaxial Angle Measuring Device and Motor

The relationship between the speed of the uniaxial angle measuring device and the voltage that controls the speed of the motor is as follows:

$$Vt\arg et = K \bullet N \quad (11)$$

where, $Vt\arg et$ is the voltage controlling motor speed (V); K is the speed scale factor formed by the combined action of motor gearbox and gear; N is the speed of optical code disk (rpm).

The conversion relationship between rpm and 0.00001 (°)/s is

$$N \bullet 360^\circ / 60S = \omega / 10^5 (^\circ) / S \quad (12)$$

where, ω is the angular velocity of the uniaxial angle measuring device (0.00001 (°)/s). 1 rpm = 6 (°)/s.

4. Software Design

4.1 Software Functions of Rotary Mechanism

The rotary mechanism takes the one-chip computer as the control system, so its function is realized through the design of the rotary control software, including:

1) Initialization of registers and variables of one-chip computer;

2) Communicate with the guidance computer, receive

DOI: https://doi.org/10.26549/met.v7i1.11641

control commands and feed back the status of the rotary mechanism;

3) Generate the synchronization signal of the uniaxial angle measuring device and receive its output angle signal;

4) Control the motor to realize the motion control command sent by the guidance computer;

5) The corresponding protection function of the rotary mechanism.

The internal interface control flow of main software components is shown in Figure 6.

The software process mainly includes:

1) Realize the initialization of the central processing unit;

2) Carry out self inspection activities for the rotary mechanism;

3) Interpret navigation commands circularly and execute corresponding actions;

4) Respond to CPU timing interrupt and external interrupt requests at any time.

The guidance computer sends various navigation commands to the rotary mechanism. The conditions for these commands are:

1) When the rotary mechanism works abnormally and needs to be corrected, an external command is sent to reset;

2) When the rotary mechanism is needed to work normally, an external command is sent to control the reciprocating rotation;

3) When the rotary mechanism needs to be stationary at a certain angle, the external sends the absolute position control command;

4) When the rotary mechanism needs to rotate at the specified speed, the external sends the speed control command;

5) When the rotary mechanism needs to rotate relative to a fixed angle and is stationary at another relevant angle, the external sends the relative position control command;

6) When the rotary mechanism needs to rotate continuously for multiple cycles in one direction according to the requirements of INS, the external sends an online calibration control command;

7) When the rotary mechanism needs to rotate to the specified angle at one time according to the requirements of INS, the external sends the initial calibration control command;

8) When the rotary mechanism needs to track the course and speed changes outside the carrier in real time to realize the reciprocating rotation relative to the geographical coordinate system, the external sends the course decoupling reciprocating rotation control command.

At any time in the above process, the rotary mechanism responds to different interrupt sources and saves new commands. After the action of the previous command is completed, execute the action of the latest command.

Various interrupt sources are as follows:

Interrupt source (1 = the highest priority) REST: reset interrupt;

Interrupt source (2 = high priority) INT0: external synchronization signal request interrupt;

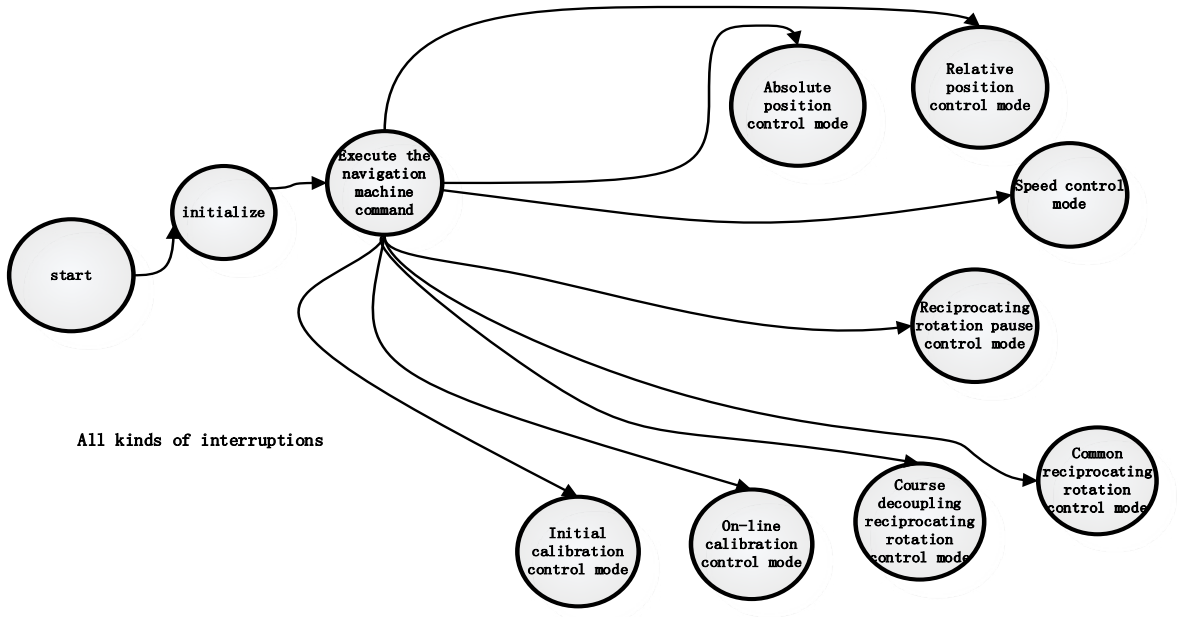

Figure 6. The internal interface of main software components.

 DOI: https://doi.org/10.26549/met.v7i1.11641

Interrupt source (3 = secondary high priority) TIMER0 OVF: timer 0 interrupt, allowing interrupt nesting;

Interrupt source (4 = medium priority) USART1 RX: interruption of communication serial port 1 receiving end;

Interrupt source (5 = secondary low priority) USART1 TX: interruption of communication serial port 1 sending end;

Interrupt source (6 = the lowest priority) USART2 RX: interruption of communication serial port 2 receiving end.

4.2 Main Program Process

The workflow of the main program of the rotation control software is shown in Figure 7. The functions that the software can realize are as follows: Receive the rate command sent by the INS, and rotate at the set rate and mode; receive the position command sent by the INS, rotate to the required position at a fixed rate, and stabilize at this position; perform the function of power-on self-test and patrol inspection during operation, and send the test results to the INS through the status word.

4.3 PID Algorithm

In the subprogram of incremental speed PID algorithm, the best effect is obtained through parameter tuning. In the subprogram of incremental speed PID algorithm, the best effect is obtained through parameter tuning, and the sequence is checked from small to large: Proportion, integral, differential. The incremental PID control structure is shown in Figure 8, and the simulation results are shown in Figure 9.

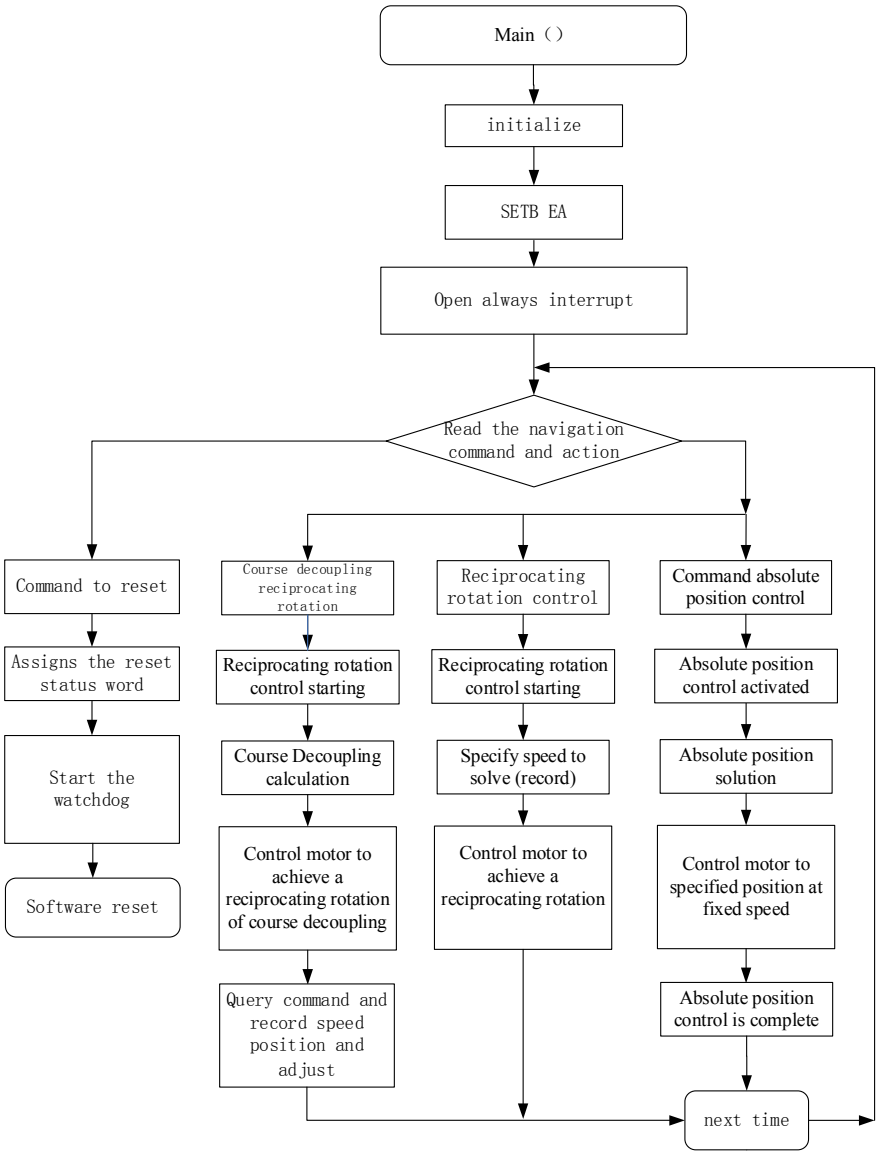

Figure 7. The workflow of the main program of the rotation control software.

DOI: https://doi.org/10.26549/met.v7i1.11641

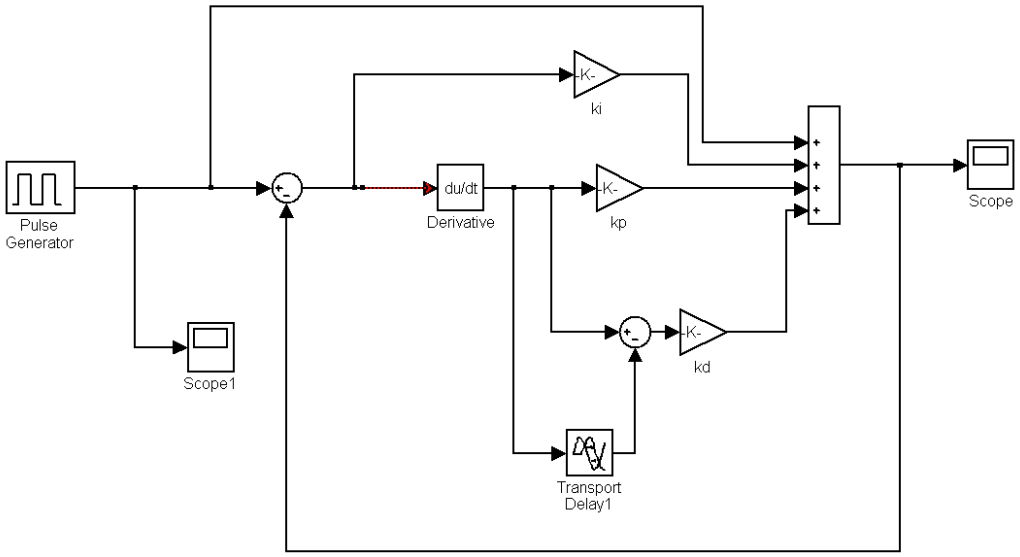

Figure 8. Incremental PID control structure.

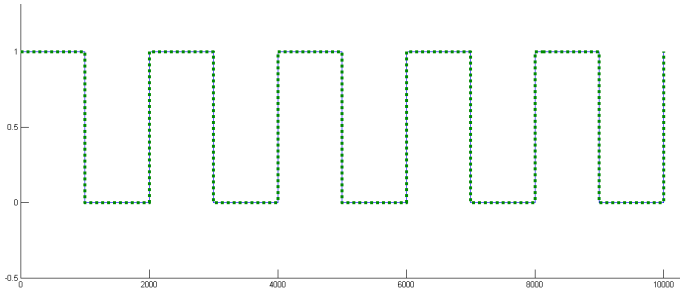

Figure 9. PID control response curve.

4.4 Motor Control

Typical motor steering switching includes three stages: accelerating for starting, uniform motion, and deceleration for braking.

When starting quickly, the analog voltage higher than the normal speed can be provided to improve the speed rising characteristic. The formula of armature starting current of motor is as follows:

$$I_{启动} = \frac{U - \Delta U}{r_{acp}} \tag{13}$$

where, U is the voltage at the debugging speed; ΔU is the saturation voltage drop of power tube, and r_{acp} is the average resistance of winding.

4.5 Control Method and Working Mode of Rotary Device

The process of rotary device control method includes:

1) Realize the initialization of the central processing unit;

2) Carry out self inspection activities for the rotary mechanism;

3) Interpret navigation commands circularly and executes corresponding actions.

The external computer sends various navigation commands to the biaxial rotating device. The conditions for these commands are:

When the rotary mechanism works abnormally and needs to be corrected, an external command is sent to reset;

When the rotary mechanism is needed to work normally, an external command is sent to control the reciprocating rotation;

When the rotary mechanism needs to be stationary at a certain angle, the external sends the absolute position control command;

When the rotary mechanism needs to track the course and speed changes outside the carrier in real time to real-

 DOI: https://doi.org/10.26549/met.v7i1.11641

ize the reciprocating rotation relative to the geographical coordinate system, the external sends the course decoupling reciprocating rotation control command;

At any time during the above steps, rotary mechanism responds to different interrupt sources and executes corresponding commands.

The rotating mechanism can provide eight working modes: absolute position control mode, relative position control mode, speed control mode, reciprocating rotation pause control mode, ordinary reciprocating rotation control mode, course decoupling reciprocating rotation control mode, online calibration control mode, and initial calibration control mode.

The functions and valid parameters of various working modes are shown in the Table 2.

The rotation control software starts running after the rotary mechanism is powered on and reset. After each power on, the rotation control software first initializes the system, and then the rotary mechanism enters the normal working state. The software performs corresponding motion control according to the received control instructions from guidance computer. At the same time, the software responds to the interruption of the synchronization signal and returns the status information of the rotary mechanism to the guidance computer.

When the DC motor stops rotating during the movement of the rotating mechanism and fails to normally receive the angular position information of the uniaxial angle measuring device for a long time, the rotary mechanism will enter the fault-safe mode, turn off the DC motor drive output, and be in a free state until the fault is eliminated.

5. Test

The calculation formula of angular rate is:

$$V_{1s计算b} = V_{1s真} + \Delta V_b = \theta_{Tb} - \theta_{Tb-1s} \tag{14}$$

where, $V_{1s真}$ and ΔV_b respectively represent the theoretical angular rate value and the actual measurement error with an interval of 1 s; θ_{Tb} and θ_{Tb-1s} respectively represent optical code disk angle of the current and 1 s ago. When $V_{1s真}$ = 10º/s, ΔV_b is usually not more than 0.3º/s. Besides, the statistical average value of angular rate with a period of 1 s can be well controlled and adjusted.

According to the environmental stress screening of strapdown inertial navigation, the rotary mechanism completes the static, vibration, impact, high and low temperature tests in turn. The test results show that the functions and performance indicators meet the task requirements. The angular rate and angle curve of the rotary mechanism of a batch are shown in Figures 10-12 respectively, and the comparison of technical indicators is shown in Table 3.

Table 2. Working mode of rotary mechanism.

No.	Mode	Function	Valid parameter
1	Absolute position control mode	The rotary mechanism can be positioned at any angle within 360°.	Angular position commanded
2	Relative position control mode	The rotary mechanism can be positioned at a relative angle within 360°.	Angular position commanded
3	Speed control mode	The rotary mechanism rotates in one direction at the specified speed.	Angular velocity commanded
4	Reciprocating rotation pause control mode	The rotary mechanism pauses during movement until the new command resumes reciprocating rotation.	/
5	Ordinary reciprocating rotation control mode	The rotary mechanism rotates back and forth with the zero position of the uniaxial angle measuring device as the center within 360°.	Angular velocity commanded; angular position commanded
6	Course decoupling reciprocating rotation control mode	The rotating mechanism rotates back and forth with the initial course angle as the center within 360° of the geographical coordinate system.	Angular velocity commanded, course angular velocity after demodulation , course angle after demodulation
7	Online calibration control mode	The rotary mechanism stops after 3 consecutive revolutions at the rate of 10(°)/s.	/
8	Initial calibration control mode	The rotary mechanism controls the absolute position to the specified angle and exits.	Angular position commanded

DOI: https://doi.org/10.26549/met.v7i1.11641

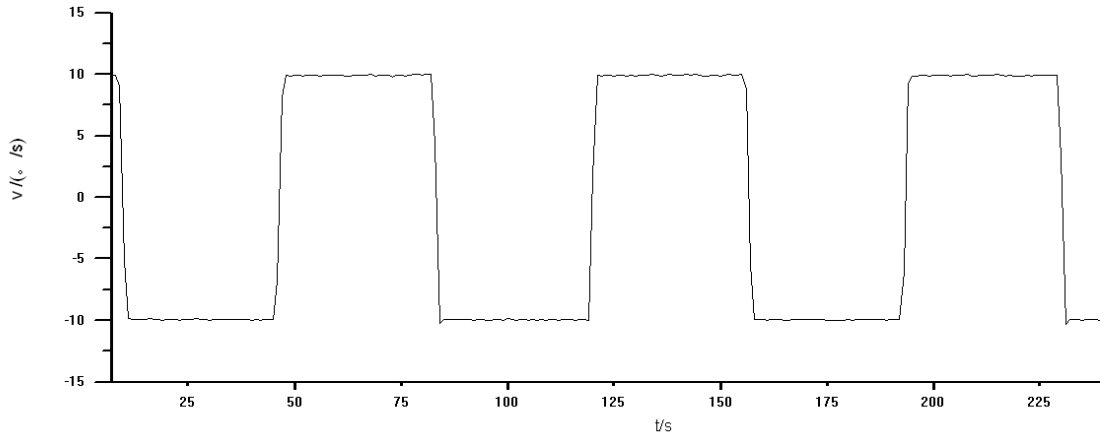

Figure 10. Graph of angular rate (10º/s).

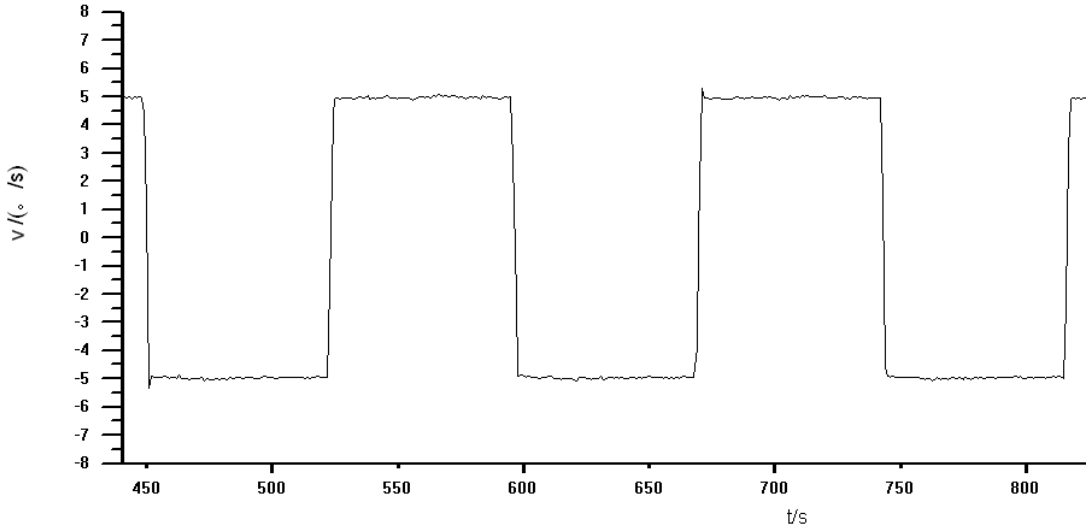

Figure 11. Graph of angular rate (5º/s).

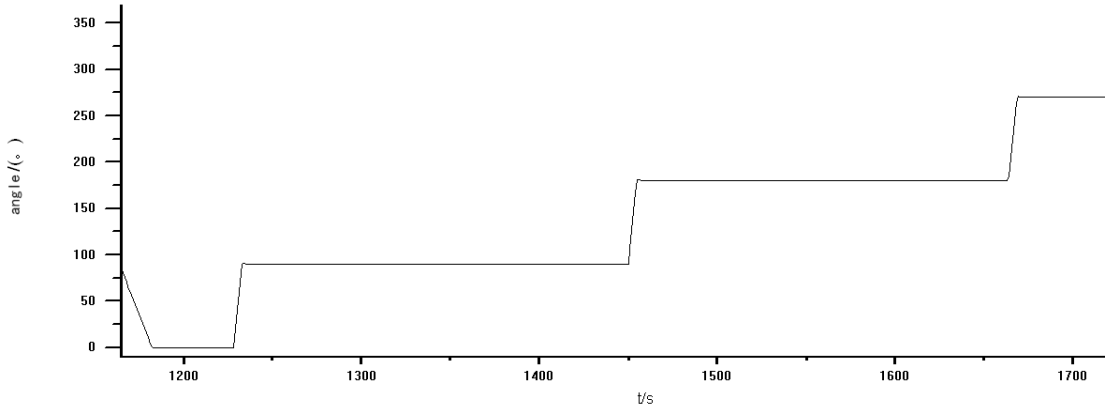

Figure 12. Graph of angle (0º, 90º, 180º, 270º).

 DOI: https://doi.org/10.26549/met.v7i1.11641

Table 3. Comparison table of technical indicators of rotary mechanism.

No.	Indicators	Requirements	Whether the design meets the requirements
1	Reciprocating rotation	Move from 0° to 360° at a specified angular rate reciprocally	Yes
2	Positioning function	Fixed at any position within the range of 0° ~ 360°	Yes
3	Angular rate range (°)/s	Not less than ±25	Yes
4	Angular rate precision	3%	Yes
5	Positioning precision (°)	0.05 (3σ)	Yes
6	Payload (kg)	5±0.4	Yes
7	Steady-state power (W)	<5	Yes
8	Transient power (W)	<7	Yes

6. Conclusions

The continuous rotation alignment has become an effective technical means to achieve high-precision of FOG inertial navigation system. This paper proposed a low-power, low-cost and medium precision scheme of uniaxial rotation navigation system. The results show that the function and performance of the rotary mechanism meet the technical requirements, which provides a strong support for giving better play to the navigation ability of the single-axial rotating FOG-SINS.

References

[1] Sun, W., 2014. Rotary modulation strapdown inertial navigation system. Beijing: Surveying and Mapping Press. pp. 5-7. (in Chinese)

[2] Titterton, D.H., Weston, J.L., 2010. Strapdown inertial navigation technology (2nd edition). Beijing: National Defense Industry Press. 10, 144.

[3] He, Ch.J., Zou, Zh.Q., Zou, Y., et al., 2016. Initial alignment of rotation-modulation strapdown inertial navigation system. Navigation Position & Timing. 3(2), 1-2. (in Chinese)

[4] Gao, Zh.Y., 2012. Inertial navigation technology. Beijing: Tsinghua University publishing house. pp. 224-253. (in Chinese)

[5] Ke, W., Qiao, H.Y., Meng, F.Q., 2012. Analysis of single-axial rotation system for the marine ring laser gyro INS. Ship Science and Technology. 34(12), 67-71. (in Chinese)

[6] Ji, Zh.N., Liu, Ch., Cai, Sh.J., et al., 2013. Improved sixteen-sequence rotation scheme for dual-axis SINS. Journal of Chinese Inertial Technology. 21(1), 46-50. (in Chinese)

[7] Xu, H.G., Guo, Y.J., Li, Zh.F., et al., 2015. Research on north-seeking precision limit of rotation-modulating FOG-SINS. Navigation Position & Timing. 3(2), 11-15. (in Chinese)

[8] Hu, Sh.S., 2016. Principles of automatic control. Beijing: Science Press. (in Chinese)

[9] Wei, Ch.G., 2006. Development of angular measuring system of testing turntable. Harbin: Harbin Institute of Technology. (in Chinese)

[10] Qi, M., Zou, J.B., Liu, Ch.J., 2007. High precision angular measuring system based on round inductosyn. Chinese Journal of Electron Devices. 30(1), 263-266. (in Chinese)

[11] Dong, J.Sh., Sun, H.Ch., Wang, H., et al., 2018. The design of A/D converter circuit with high resolution integral output. Navigation Position & Timing. 5(1), 93-94. (in Chinese)

[12] Liu, J.K., 2016. Matlab simulation of advanced PID control. Beijing: Publishing House of Electronics Industry. (in Chinese)

[13] Liu, F.Q., Zhang, G.Y., Wang, L.Y., et al., 2008. Control system for two-axis turntable based on single chip microcomputer. Journal of Changchun University of Science and Technology. 31(4), 87-90. (in Chinese)

[14] Kim, J.Y., Kim, I.S., Lee, H.N., et al., 2001. A study on the feedback system of ultra precision positioning apparatus using laser inrergerometer. Insdutrial Electronics. Pusan, KOREA:IEEE int symp. 1, 596-601.

[15] Zhang, L.D., Lian, J.X., Wu, M.P., et al., 2012. Research on yaw angle isolation method of inertial navigation system based on single-axis rotation. Chinese Journal of Scientific Instrument. 33(6), 1247-1250. (in Chinese)

[16] Gao, Y.B., Guan, L.W., Wang, T.J., 2013. Compensation for inclination angle deviation of single-axis rotation modulation SINS. Journal of Chinese Inertial Technology. 21(4), 446-448. (in Chinese)

DOI: https://doi.org/10.26549/met.v7i1.11641

SYNERGY PUBLISHING PTE. LTD.

Modern Electronic Technology

http://www.advmodoncolres.sg/index.php/amor/index

Dynamic Prediction Method for Valuable Spare Parts Demand in Weaponry Equipment Based on Data Perception

Weiyi Wu* **Yunxian Jia** **Yangyang Zhang** **Bin Liu**

Shijiazhuang Campus, Army Engineering University, Shijiazhuang, Hebei, 050003, China

ARTICLE INFO

Article history
Received: 5 January 2023
Revised: 22 January 2023
Accepted: 15 March 2023
Published Online: 19 April 2023

Keywords:
Data perception
Missile equipment
Spare part
Demand
Dynamic prediction

ABSTRACT

Missile is an important weapon system of the army. The spare parts of missile equipment are significant effect on military operations. In order to improve the mission completion rate of missile equipment in wartime, this paper introduces data sensing method to forecast the demand of valuable spare parts of missile equipment dynamically. Firstly, the information related to valuable spare parts of missile equipment was obtained by data sensing, and the sample size was determined by Bernoulli uniform sampling probability. Secondly, according to the data quality of multi-source and multi-modal, the data requirement for dynamic demand prediction of valuable spare parts of missile equipment was obtained. Finally, according to the characteristics of the spare parts, the life of the spare parts was predicted, realizing the dynamic prediction of the demand for valuable spare parts of missile equipment. The results show that the demand of valuable spare parts of missile equipment can be predicted dynamically by using this method, the accuracy is higher than 95%, and the real-time performance is more excellent.

1. Introduction

Spare parts are the material basis in the support resources of surface-to-air missile weapons and equipment. The allocation and ordering of spare parts are very important for the support of weapons and equipment and directly affect the integrity of equipment and the combat effectiveness of troops. A military missile equipment consists of about 3 million to 6 million parts, including a large number of valuable parts [1]. The supply support of such a large number of valuable spare parts is an important link of combat effectiveness producation, so it is necessary to study and discuss the demand forecasting method of valuable spare parts of missile equipment based on data management and analysis technology. This paper studies the dynamic prediction method of intermittent mechanical spare parts demand based on data perception, and applies the data sensing method to the dynamic prediction of missile equipment valuable spare parts demand, which can improve the scientific rationality of missile equipment maintenance spare parts inventory.

2. Demand Data Perception Method Based on Data Quality

The valuable spare parts of missile equipment possess intermittent characteristics. The dynamic fault information of valuable spare parts can be obtained effectively through data sensing method, and the demand prediction can be realized using the fault information.

**Corresponding Author:*
Weiyi Wu,
Shijiazhuang Campus, Army Engineering University, Shijiazhuang, Hebei, 050003, China;
Email: weiyi1019@163.com

 DOI: https://doi.org/10.26549/met.v7i1.11941

2.1 Data Acquisition

When collecting large-scale data, in order to truly reflect the fault information of missile equipment, the sensing area is usually divided into several disjoint sub regions, and the data are collected in each sub area to reflect the change of the whole perception area.

The missile equipment fault information Z is divided into *K* disjoint sub regions, which are expressed as $Z=\{z_1,z_2,\cdots,z_K\}$. Due to the large number of sub regions, if the heterogeneous data sources of each sub region all send their sensing data to the data processing center for upper level applications, the data transmission volume is too large, and finally a large number of data distortion is caused by data congestion [7,8]. In the process of data acquisition, the data quality information reflects the accuracy, integrity and consistency of the data. The higher the data quality is, the more reliable the decision-making results can be obtained by using these data. The main idea of the algorithm is as follows.

According to the accuracy requirements $\varepsilon(\varepsilon\geq 0)$ and $\delta(0\leq\delta\leq 1)$ given by users, the Bernoulli uniform sampling algorithm is used to perform (ε,δ)-approximation on the multi-source and multi-modal data quality of the overall perception data [9], and the sampling probability *p* required by the users is obtained. Finally, in order to save the network resources as much as possible, *pK* data sources are selected for data transmission.

Supposing the start time of *K* disjoint sub regions is $t_s t_s$, and its multi-source, multimodal data set is $S=\left\{D_{t_s}^{(1)},D_{t_s}^{(2)},\cdots,D_{t_s}^{(K)}\right\}$, and the corresponding data quality set is $DQ=\{q_1,q_2,\cdots,q_k\}$. Each multi-source and multi-modal data quality information includes accuracy, integrity and consistency. Then the data quality information of the whole missile equipment fault information area is the weighted average value of the each sub region data quality [10]:

$$Avg(DQ)=\sum_{i=1}^{K}w_i q_i / \sum_{i=1}^{K}w_i \tag{1}$$

where $W_Z=\{w_1,w_2,\cdots,w_K\}$ are the weights of the *K* sub regions. The weight of each sub region is usually unchanged, or the small change of the weight has little influence on the weight sum, so the weight sum is regarded as a constant.

2.2 Bernoulli Uniform Sampling Probability Determination

In order to obtain the accurate demand for valuable spare parts of missile equipment, it is necessary to determine the specific value of the data sample. In this paper, Bernoulli uniform sampling probability method is used to calculate the appropriate sample size.

Assuming that $\overline{I}$ is the estimated value of the actual demand *I* for valuable spare parts. For any actual probability $\varepsilon(\varepsilon\geq 0)$ of missile spare parts failure and the sensor sensing failure probability $\delta(0\leq\delta\leq 1)$, if the missile spare parts demand meet $\Pr\left(\left|\overline{I}-I\right|I\geq\varepsilon\right)\leq\delta$, then the $\hat{I}$ is called approximate estimation of *I*, where $\Pr(X)$ is the occurrence probability of event *X*. The specific process is shown in the following figure:

If the sampling probability of data quality information set DQ is p, then the approximate value of multi-source and multimodal data quality is as follows:

$$Avg\left(\overline{DQ}\right)=\frac{\sum_{i=1}^{K}w_i q_i\cdot x_i}{p\sum_{i=1}^{K}w_i} \tag{2}$$

where the binary random variable x_i indicates whether the missile fault data information in the sub area z_i is extracted, and the extracted value is 1, otherwise it is 0. That is, random variables x_i obey two-point distribution, and $\Pr(x_i=1)=p$. In addition, the x_i of different regions are independent. The sensing fault data of missile equipment is $E(x_i)=p$, and its binomial distribution variance is $E(x_i)'=p(1-p)$.

The unbiased estimation $Avg\left(\overline{DQ}\right)$ of missile spare parts data quality information set can be obtained through Bernoulli uniform sampling [11-13]:

$$E\left(Avg\left(\overline{DQ}\right)\right)=Avg(DQ) \tag{3}$$

According to the definition of $Avg\left(\overline{DQ}\right)$:

$$E\left(Avg\left(\overline{DQ}\right)\right)=E\left(\sum_{i=1}^{K}w_i q_i\times x/p\sum_{i=1}^{K}w_i\right) \tag{4}$$

Since the the x_i of sub regions are independent, so:

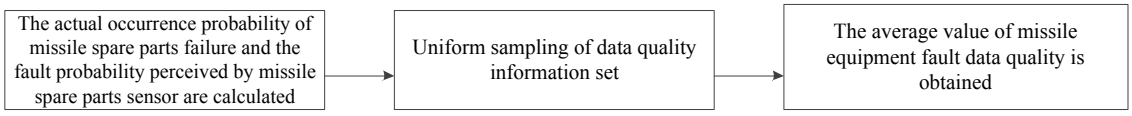

Figure 1. Quality average value solution of missile equipment fault data.

DOI: https://doi.org/10.26549/met.v7i1.11941

$$E\left(Avg\left(\overline{DQ}\right)\right)=\left(\sum_{i=1}^{K}w_iq_i/p\sum_{i=1}^{K}w_i\right)E\left(x_i\right)=\left(\sum_{i=1}^{K}w_iq_i/p\sum_{i=1}^{K}w_i\right)\cdot p=Avg\left(DQ\right) \tag{5}$$

$Avg\left(\overline{DQ}\right)$ is unbiased estimation of data quality accurate weighted mean $Avg\left(DQ\right)$. According to the central limit theorem, when the sample size is greater than or equal to 30, $Avg\left(\overline{DQ}\right)$ obeys the normal distribution, and the expectation is $E\left(Avg\left(\overline{DQ}\right)\right)=Avg\left(DQ\right)$ and the variance is $Var\left(Avg\left(\overline{DQ}\right)\right)$. In the environment of large-scale sensor network, when sampling the service data obtained by sensor, the required sample size will be far greater than 30 under very low precision requirements. So it is true that $Avg\left(\overline{DQ}\right)$ obey approximate normal distribution. At this condition, $E\left(Avg\left(\overline{DQ}\right)\right)$ is the appropriate sample size of valuable spare parts for missile equipment.

2.3 Data Acquisition Method Based on Multi-source and Multimodal Data Quality

The calculation steps of data acquisition method based on multi-source and multimodal data quality are as follows:

Input: weight W_Z, data quality $Sup\left(DQ\right)$ and $Inf(DQ)$

Output: Perceptual data set D_s to be transmitted

1) Initialize $W_{\max}=0$, $Sum\left(W_Z\right)=0$

2) For each w_i in W_Z Do

3) $Sum\left(W_Z\right)+=w_i$

4) If $w_i>W_{\max}$ then

5) $W_{\max}=w_i$

6) Calculate the sampling probability

7) $p=\dfrac{Sup\left(DQ\right)W_{\max}\phi_{\delta/2}^2}{Sup\left(DQ\right)W_{\max}\phi_{\delta/2}^2+Inf\left(DQ\right)Sum\left(W_Z\right)\varepsilon^2}$

8) For each sensor aera $z_i\in Z$ Do

9) Generate a random number s in range [0,1]

10) If $r<p$ then

11) Send its data D_i to the data center

12) $D_s\leftarrow\left\{D_i\right\}$

13) Return D_s

Firstly, the maximum weight $W_{\max}$ and the weights sum $Sum\left(W_Z\right)$ are obtained based on the weight W_Z of each sub region. After that, the upper bound $Sup\left(DQ\right)$ and the lower bound $Inf\left(DQ\right)$ of data quality are given. Generally, the upper bound is taken as 1, and the lower bound is given by the users according to their specific requirements [14].

After the sampling probability is determined, the data processing center performs Bernoulli uniform sampling in the K sub regions. The specific steps are as follows: The data processing center generates a random number r between [0, 1] for each sub region. If r is less than or equal to the sampling probability p, the perceived data $D_i\left(1\le i\le K\right)$ of the region is the data needed for dynamic demand prediction of valuable spare parts, otherwise the sensing data in this area is invalid.

3. Results

In order to test the validity of the dynamic prediction method in this paper, the dynamic demand prediction of 12 intermittent key valuable spare parts for an anti-tank missile equipment is simulated based on the Matlab platform. The demand of 12 kinds of missile equipment spare parts from 2013 to 2018 is counted. The statistical results are shown in Table 1.

The historical fault interval is extracted from the maintenance record of 12 valuable spare parts of missile equipment each year. The historical data is shown in Table 2.

In order to obtain accurate spare parts demand, the fault data of missile equipment spare parts are grouped based on the above data. The main shaft of the missile belongs to mechanical wear parts, which is prone to a large number of faults in the running stage. The time between failures usually conforms to Weibull distribution and exponential distribution, and few obey lognormal distribution and normal distribution. In this paper, the scatter diagram of fault data is used to judge its distribution model, and then the parameter solution and fitting verification are carried out. The fault interval time is sorted and grouped within [0, 4200] hours. The number of groups is determined by formula (6).

$$Z_p=1+3.3ln\mathrm{R} \tag{6}$$

The number of non-truncated fault data is 81, and the reliability *n* of system components is 8. R is the wartime maintenance replacement rate. According to the above formula, the grouping and sorting table is as follows.

 DOI: https://doi.org/10.26549/met.v7i1.11941

Table 1. Demand data of 12 types of missile equipment spare parts from 2013 to 2018.

Spare part number	2013year/N	2014year/N	2015year/N	2016year/N	2017year/N	2018year/N
1	48	51	53	59	61	65
2	62	68	69	72	76	77
3	56	58	59	61	68	69
4	72	75	76	78	79	81
5	76	78	79	82	83	85
6	49	51	53	58	62	68
7	68	76	79	82	86	91
8	32	35	38	41	48	52
9	66	68	71	72	76	79
10	81	83	86	91	94	95
11	46	48	51	58	62	68
12	52	57	59	61	64	69

Table 2. Failure interval of each spare part.

Spare part number	Time between failures
1	756.5,1025.3,1125.6,925.3,1125.5,1025.6,1142.6,1326.8,1425.9,1042.6,1125.6,1042.6,836.5,912.5
2	835.6,905.2,912.5,1025.6,1125.6,963.5,1124.5,1134.5,1241.5,1052.6,1325.1,1254.6,915.2
3	948.5,985.6,1056.6,1125.4,1264.5,935.5,846.5,923.5,1235.6,1325.5,1154.6,1234.5,1354.5,942.3,879.6,845.6,1125.6
4	1052.6,1125.3,1264.5,1325.4,1025.4,1059.5,1134.6,1425.9,945.5,1352.4,1254.6,1954.6,876.5,905.6
5	912.5,1054.6,1129.5,1325.4,942.6,984.5,986.5,1025.4,1165.8,1241.2,1305.6,1254.2,1326.8,945.2,948.6,1058.5,1157.6
6	1025.6,1152.4,1305.8,978.5,962.5,1025.6,1254.6,1305.2,987.5,996.5,1251.2,1325.6,945.5,1254.3,1052.6,1321.2,978.5,864.5,894.5,1025.6,1124.6
7	945.5,1056.2,1354.6,1052.6,1364.5,1125.6,1254.6,1356.5,1428.2,1243.6,1352.3,985.6,845.6,1024.5,1125.6,1325.5,945.2,845.6,795.6,1025.6
8	1025.6,1125.6,1245.6,1254.6,1285.6,1297.5,1246.5,1325.1,1154.2,1536.2,1052.6,1024.5,985.6,1034.2,1065.5,1289.5,1294.5,1234.2,1185.6,1145.6,1085.6,1125.4
9	985.6,894.52,1025.6,1254.6,1325.6,1058.6,1125.5,1245.6,1352.5,1024.6,985.6,998.65,1024.5,1054.3,1156.3,1284.6,1325.6,1152.6,1285,6,1045.2,1326.5,1205.3,986.5
10	1025.3,1125.4,1264.5,1305.3,1264.5,1305.6,1325.6,1156.5,985.6,975.6,1125.5,1234.5,1265.2,1352.6,1242.6,1325.2,1425.3,1025.6
11	952.6,976.5,1025.3,1156.5,1215.6,1305.8,1164.5,1265.5,1305.2,984.5,1058.6,1152.6,1245.6,1325.2,985.6,994.5,1025.6,1152.6,1143.5,1253.6,1246.5,1352.6,1025.6
12	1025.6,1125.6,1165.5,1325.4,952.6,945.3,865.6,786.5,1025.6,1152.4,1168.5,1262.3,1254.3,1325.3,1152.3,1085.3,1125.3,1231.2,1302.5

DOI: https://doi.org/10.26549/met.v7i1.11941

Table 4. Fault interval time sorting table.

Upper limit	Lower limit	Value in the group	Frequency number	Frequency	Accumulation
0	600	300	21	0.2593	0.2593
600	1200	600	16	0.1975	0.4568
1200	1800	9000	10	0.1235	0.5802
1800	2400	1200	9	0.1111	0.6914
2400	3000	1500	8	0.0988	0.7901
3000	3600	1800	8	0.0988	0.8889
3600	4200	2100	7	0.0864	0.9753
4200	4800	2400	2	0.0247	1.0000

The observation value $K(t)$ of probability density is calculated as follows:

$$K(t) = \frac{M_i}{M \cdot \Delta t} \tag{7}$$

where M_i is the number of fault intervals in each group, M is the total number of fault intervals, Δt is the group spacing. Through the Matlab simulation calculation of the data, the dynamic prediction results of the demand for 12 valuable spare parts in 2019 are obtained. Compared with wavelet analysis method and GM method, the results are shown in Figure 1.

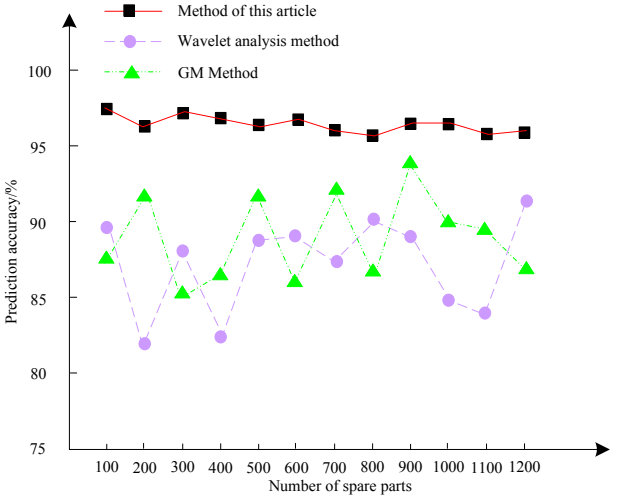

Figure 1. Comparison of prediction accuracy of different methods.

The prediction accuracy is transformed into the accuracy rate of spare parts fault identification. If the spare parts that have faults are identified, they need to be replaced, and then the prediction accuracy rate of valuable spare parts demand will become high.

According to the experimental results in Figure 1, the method accuracy is different for different spare parts numbers. When the number of spare parts is 100, the prediction accuracy of wavelet analysis method is 87%, that of GM method is 89%, and that of this proposed method is 97%. When the number of spare parts increases to 800, the prediction accuracy of wavelet analysis method is 90%, that of GM method is 86%, and that of this proposed method is 96%. The prediction accuracy of the method proposed in this paper is high, and it can accurately predict the demand of valuable spare parts for missile equipment.

The prediction time of the valuable spare parts demand of 12 intermittent missile equipment is dynamically predicted with this method, and the results are compared with wavelet analysis method and GM method, shown in Figure 2.

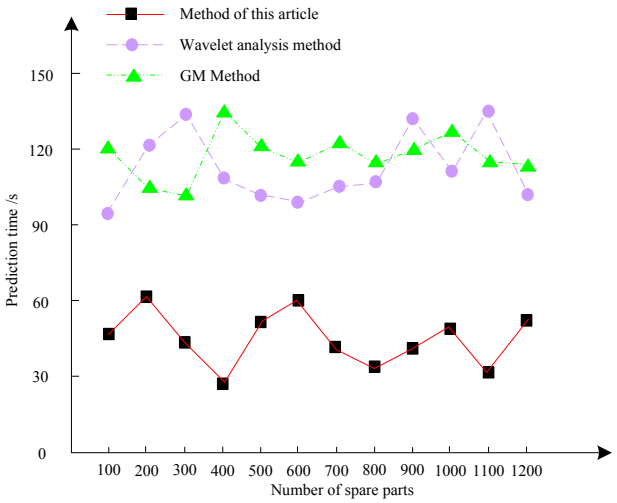

Figure 2. Comparison of prediction time of different methods.

According to the experimental results in Figure 2, when the number of spare parts is 200, the prediction time of wavelet analysis method is 120 s, that of GM method is 110 s, and that of the method in this paper is 60 s. When the number of spare parts increases to 1200, the prediction time of wavelet analysis method is 115 s, that of GM method is 110 s, and that of the method in this paper is 58 s. The prediction time of the method proposed in this paper is short and the prediction efficiency is high. The experimental results verify the real-time performance of the proposed method.

4. Discussions

Missile equipment is a complex electromechanical system. Fault prediction and inventory control of maintenance spare parts are the key factors affecting the combat effectiveness of missile equipment. The data sensing method is applied to the dynamic prediction of intermittent mechanical spare parts demand. This paper forecasts the demand of valuable spare parts of missile equipment

DOI: https://doi.org/10.26549/met.v7i1.11941

based on data perception method. The main conclusions are as follows:

(1) In this paper, the new method is used to study the demand law of spare parts design and the simplified workload, and the demand forecast in the spare parts management is mainly studied.

(2) Due to the lack of data samples, the simulation of equipment use and maintenance process is proposed to obtain fitting samples. The method to determine the sample size makes the simulation process universal, which can effectively avoid multiple parameter estimation and hypothesis testing, and reduce the sampling difficulty of complex probability distribution. The research designs the definite time interval combining with specific problems, and obtains excellent results.

(3) The research results in this paper can be applied to the optimal allocation of spare parts in the ground to air system. According to the actual problems, the relevant parameters of spare parts demand prediction can be obtained, and the optimal inventory optimization result can be obtained by using data sensing method to solve the demand of missile spare parts dynamically.

5. Conclusions

In the dynamic prediction of the demand of valuable spare parts, the method based on data perception is introduced to forecast the demand of valuable spare parts dynamically. The basic data of dynamic prediction of the demand for valuable spare parts is obtained by data perception method based on data quality, and the sample size of valuable spare parts is determined by Bernoulli uniform sampling probability. According to the material characteristics of spare parts, the life prediction of missile equipment valuable spare parts is realized. Finally, valuable spare parts are taken as experimental objects to test the effectiveness of the dynamic prediction method. The results show that the method can be applied to the dynamic prediction of valuable spare parts of actual missile equipment, and provide the basis for the integrated support of missile equipment.

References

[1] Xiong, Y., Qi, Y.L., 2019. Capability and equipment prediction analysis of missile defense system in the United States. Tactical Missile Technology. 193(01), 39-42.

[2] Zuo, W.B., Zhao, Y.J., He, L., 2018. Spare parts demand forecast method in wartime for surface air defense group. Journal of Academy of Military Transportation. (02), 25-28.

[3] Wang, W.Sh., Liu, Ch.Y., Xu, C.X., et al., 2018. Design for a fault diagnosis and prognosis system of missiles. Journal of Naval Aeronautical and Astronautical University. 33(5), 486-492.

[4] Qiu, L.J., Fu, L.Y., Dong, Q., et al., 2018. Research on spare demand prediction based on support vector machine by genetic algorithm optimization parameter. Journal of Sichuan Ordnance. 39(4), 88-91.

[5] Zhao, J.Zh., Xu, T.X., Li, H.J., et al., 2014. Combination forecasting of missile equipment spare parts demand based on wavelet analysis. Acta Electronica Sinica. (003), 417-423.

[6] Jiliang, T.U., Hong, Y.U., Song, Y.U., et al., 2019. Aircraft spare parts requirement forecasting model based on performance support analysis. Journal of Naval Aeronautical and Astronautical University. 34(04), 356-362.

[7] Zhao, X., Wang, K., Su, G.Y., et al., 2018. Status analysis and trend forecast of global missile trading market. Tactical Missile Technology. (2), 16-25.

[8] Zhao, J.Y., Wang, X., Liu, X., 2019. Corrosion life prediction of naval missile structure parts. Equipment Environmental Engineering. 16(4), 51-54.

[9] Liu, Y., Zhang, Q., Fan, Z.P., et al., 2019. Maintenance spare parts demand forecasting for automobile 4S shop considering weather data. IEEE Transactions on Fuzzy Systems. 27(5), 943-955.

[10] Nair, M.K.S., Mohamad, H., Jamil, H.A., et al., 2018. Forecasting military vehicle spare parts requirement using neural networks followed by application of tacit knowledge. International Journal of Engineering & Technology Sciences. 7(29), 13-17.

DOI: https://doi.org/10.26549/met.v7i1.11941

SYNERGY PUBLISHING PTE. LTD.

Modern Electronic Technology

http://www.advmodoncolres.sg/index.php/amor/index

Application of PCA Numalgorithm in Remote Sensing Image Processing

Hong Dai*

School of Computer and Information Engineering, Shanghai Second Polytechnic University, Shanghai, 201209, China

ARTICLE INFO

Article history
Received: 5 February2023
Revised: 8 March 2023
Accepted: 10 March 2023
Published Online: 19 April 2023

Keywords:
PCA numerical algorithm
Remote sensing image processing
Multi-spectral image

ABSTRACT

A numerical algorithm of principal component analysis (PCA) is proposed and its application in remote sensing image processing is introduced: (1) Multispectral image compression; (2) Multi-spectral image noise cancellation; (3) Information fusion of multi-spectral images and spot panchromatic images. The software experiments verify and evaluate the effectiveness and accuracy of the proposed algorithm.

1. Introduction

Image processing is a technology of enhancing, pressing, correcting and identifying the images obtained by space remote sensing device and earth resource exploration platform to extract thematic information. It is a basic part of the whole remote sensing observation process [1]. Principle Component Analysis (PCA), also known as K-L transformation, is a multi-dimensional orthogonal transformation based on statistical characteristics. It is the best transform to remove the correlation between data, but its operation amount is large. This paper proposes a fast PCA numerical algorithm implemented in the computer, and realizes its application in the remote sensing image processing from three aspects through the software experiment: (1) Multi-spectral image compression. (2) Multi-spectral image noise cancellation. (3) Information fusion of multi-spectral images and spot panchromatic images.

2. The PCA Numerical Algorithm

Let an image sequence have n pictures, each graph size is k = M N (M-number of rows; N-number of columns), stack these images, and store the pixel value of each graph in a one-dimensional array, then the image sequence is represented by a two-dimensional array X, and an n-dimensional column vector X_i represents the set of all pixel values on position i, i.e.:

$$\boldsymbol{X_i} = [\mathbf{x}_{1i}, x_{2i}, \ldots, x_{ni}]^T \quad (1)$$

is

$$X = [\, X_1 \ldots \boldsymbol{X_k}]$$

The steps of transform X with PCA numerical algorithm are as follows:

(1) Calculates the mean vector m of X_X and the covari-

**Corresponding Author:*
Hong Dai,
School of Computer and Information Engineering, Shanghai Second Polytechnic University, Shanghai, 201209, China;
Email: daihong419@163.com

 DOI: https://doi.org/10.26549/met.v7i1.12317

ance matrix, C_X.

The mean vector of X is:

$$\boldsymbol{m}_X = E[X] = \frac{1}{k}\sum_{i=1}^{k} = X_i \tag{2}$$

The covariance matrix of X is:

$$\boldsymbol{C}_X = E[(X - m_X)(X - m_X)^T] = \frac{1}{k}\sum_{i=1}^{k}(X_i - \mathbf{m}_X)$$

$$(X_i - \mathbf{m}_X)^T = \begin{bmatrix} \boldsymbol{C}_{11} & \boldsymbol{C}_{12} & \ldots & \boldsymbol{C}_{1n} \\ \boldsymbol{C}_{21} & \boldsymbol{C}_{22} & \ldots & \boldsymbol{C}_{2n} \\ \ldots & \ldots & \ldots & \ldots \\ \boldsymbol{C}_{n1} & \boldsymbol{C}_{n2} & \ldots & \boldsymbol{C}_{nn} \end{bmatrix} \tag{3}$$

among C_{ij} (i,j=1,2,…n) reflects the correlation between pixels i and j. If the different pixels are unrelated, then C_X for diagonal arrays. C_X is the real symmetric array, hence the orthogonal matrix A, making C_X hierarchization, i.e.:

$$\Lambda = A^T \boldsymbol{C}_X A = \begin{bmatrix} \boldsymbol{\lambda}_1 & \mathbf{0} & \ldots & \mathbf{0} \\ \mathbf{0} & \boldsymbol{\lambda}_2 & \ldots & \mathbf{0} \\ \ldots & \ldots & \ldots & \ldots \\ \mathbf{0} & \ldots & \ldots & \boldsymbol{\lambda}_n \end{bmatrix} \tag{4}$$

where the element on the diagonal is a C_X. The eigenvalue of, and sets the $\lambda_1 \geq \lambda_2 \geq \ldots \geq \lambda_n$, A for C_X eigenvector matrices corresponding to these eigenvalues.

(2) Principal component transformation [2]

Let the matrix y be:

$$\boldsymbol{y} = \boldsymbol{A}(\boldsymbol{X} - \boldsymbol{m}_X) \tag{5}$$

Formula (5) is the principal component transformation of X. It tiably that the covariance matrix of y

$$\boldsymbol{C}_y = E[(y - m_y)(y - m_y)^T] = AC_X\boldsymbol{A}^T \tag{6}$$

Certificate: The mean value of y: $m_y = E[A(X - m_X)] = A E[X] - Am_X = \boldsymbol{Am_X - Am_X = 0}$

The covariance array of y:

$$\boldsymbol{C}_y = E[(y - m_y)(y - m_y)^T] = E[yy^T] - m_y\boldsymbol{m}_y^T = E[yy^T] = E[A(X - m_X)(X - m_X)^T\boldsymbol{A}^T] = A\,C_X\boldsymbol{A}^T.$$ By proof.

It is thus clear that C_y is a diagonal array, and the element on its main diagonal is called C_X. The eigenvalues of y column vectors are not correlated with each other. The principal component transformation can therefore remove the correlation between the data.

(3) Numerical algorithm for finding the eigenvector matrix A

In order to find A in a fast iterative way on the computer, the ancient and elegant comparable algorithm of solving the eigenvalue and the eigenvector of the real symmetric matrix is adopted first. The solution process is: At each iteration, in C_XSelect the element with the largest absolute value, and set it in column q of line p (let q> p), using the n-order rotation matrix R corresponding to the position$^{(k)}$To C_XOrthogonal similarity transformation, i.e.

$$\boldsymbol{C}_X^{(k)} = [R^{(k)}]^T\boldsymbol{C}_X^{(k-1)}\boldsymbol{R}^{(k)} (k = 1,2,\ldots\ldots) \tag{7}$$

among $C_X^{(0)} = C_X$, $R^{(k)}$The element $r_{pp}^{(k)} = \cos\theta$, $r_{qq}^{(k)} = \cos\theta$, $r_{pq}^{(k)} = -\sin\theta$, $r_{qp}^{(k)} = \sin\theta$, $r_{ij}^{(k)} = 0 (i, j \neq p,q)$, $r_{ii}^{(k)} = 1 (i \neq p,q)$.

1) If $r_{pp}^{(k-1)} - r_{qq}^{(k-1)} = 0$, (i) When $r_{pp}^{(k-1)} > 0, \theta = \pi/4$. (ii) When $r_{pp}^{(k-1)} < 0$, $\theta = -\pi/4$.

2) If $r_{pp}^{(k-1)} - r_{qq}^{(k-1)} = 0$, which is determined by the following equation:

$$tg2\theta = \frac{2r_{pq}^{(k-1)}}{r_{pp}^{(k-1)} - r_{qq}^{(k-1)}} \ (|\theta| < \pi/4) \tag{8}$$

Each passing orthogonal similarity transformation, C_X. The sum of diagonal element squares increases by $2r_{pq}^2$. Again and again to C_X, Transform according to equation (7) until $|r_{pq}^{(k)}| < \varepsilon$ (p =q, a small positive number), you can be C_X. Gradually transform, for the diagonal array. The element on the diagonal in this diagonal array is a C_X. The eigenvalues of, the successive orthogonal similarity transformation matrix $R^{(k)}$. The product is C_X. The eigenvector matrix of A:

$$\boldsymbol{A} = \boldsymbol{R}^{(1)}\ldots R^{(k)} \tag{9}$$

Because of the ancient and elegant comparable method, it takes a time consuming to find the largest absolute value of the off-diagonal element every time, using the "pass method" [3]. Improvement: First, calculate C_X, the sum of off-diagonal squares and root are:

$$v_0 = [\sum_{i<j}(\boldsymbol{C}_{ij})^2]^{1/2} = 2 \tag{10}$$

Set Level 1 $v_1 = v_0 In / n$, as described in C_XScan by line in non-diagonal elements, if $|C_{ij}| > v_1$. To use the rotation matrix $R^{(k)}$To C_XOrthogonal similarity transform, otherwise "pass" and undergo multiple scans until all off-diagonal elements are less than v_1; Set pass 2 $v_2 = v_1$For / n, the above procedure is repeated until all off-diagonal elements are less than v_2; By analogy, through a series of passes $v_2, v_3, \ldots, v_r$. Until you meet the requirements of: $v_r \leq \rho v_1$, where is the accuracy requirement. The clearance method accelerates the convergence process of the Jacobian method.

(4) Error analysis

Inverse transformation formula through the principal component transformation: $X = A^T\boldsymbol{y} + \boldsymbol{m}_X$. Accurately rebuild the X. To compress the redundant information in this n image, then the m eigenvector A corresponding to the first m largest eigenvalues of y is taken$_1 \sim A_m$. To approximately reconstruct X, because $A_1 \sim A_m$. The main information in X is concentrated. The reconstruction formula is:

DOI: https://doi.org/10.26549/met.v7i1.12317

$$X_s = y\sum_{i=1}^{m} {}_i A_i + m_X \quad (11)$$

Then X and X_s The total mean squared error ems between is:

$$e\ ms = E[(X - X_s)(X - X_s)^{T}] = \sum_{j=m+1}^{n} \lambda_j = \frac{1}{MN}\sum_{i=1}^{M}\sum_{j=1}^{N}(X - X_s)^2 \quad (12)$$

The number of feature vectors, m, is selected according to the error requirement.

3. PCA Numerical Algorithm for Remote Sensing Image Compression

Remote sensing multi-spectral images have the characteristics of large data volume and high dimension, and massive data needs huge storage space [3]. The TM (thematic mapping instrument) multispectral images obtained by Landsat (Landsat) include seven bands: TM1 (visible blue light), TM2 (visible green light), TM3 (visible red light), TM4 (near infrared short wave), TM5 (near infrared medium wave), TM6 (thermal infrared) and TM7 (near infrared long wave) [2]. The correlation between the individual band images is very high, thus offering the possibility for image compression.

PCA numerical algorithm image compression experimental environment is a 256M memory of the Pentium computer and Matlab7.0 software. Data were obtained from a set of images from the Landsat satellite TM1 to TM7 band in the Colorado River, USA. Each drawing measures it at 512,512. Figure 1(a) was transformed by the PCA numerical algorithm. The first 3 principal component images are shown in Figure 1(b). The front m (m =1~7) main component images to approximately reconstruct the original image sequence. The proportion, compression ratio and reconstruction errors of their ground information are shown in Table 1, C_y the seven feature values are: ${}_1$=4889.90, λ_2=164.74, λ_3= 95.24, λ_4=49.08, λ_5=19.61, λ_6=10.57, λ_7=5.00. Visible that the first 3 principal component images already include:

$(\lambda_1+\lambda_2+\lambda_3)/\sum_{i=1}^{7}\lambda_i$ = has 98.39% of the ground object information and the data volume is compressed to 42.9%. A 77 matrix C was solved in the experiments by Jacobi clearance$_X$The eigenvalues and eigenvectors, in the accuracy requirements of =10, respectively^{-2}, 10^{-3}And 10^{-4}. Next, the number of iterations was 4, 5, and 6 times, respectively.

And its principal component images: (a) TM1~7 band images (b) Top 3 primary component images).

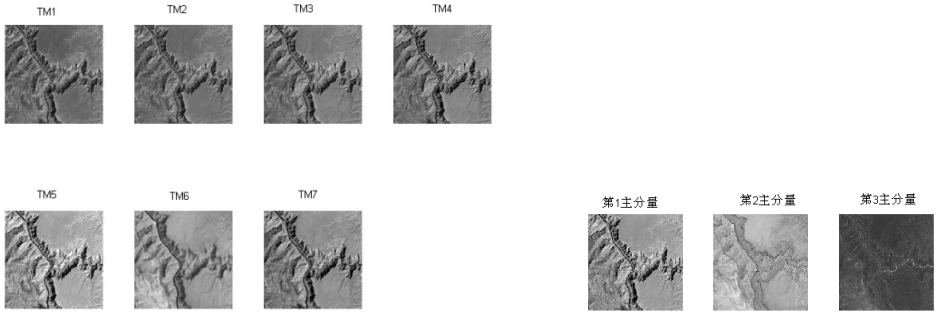

(a) (b)

Figure 1. A TM multispectral image of the Colorado River

Table 1. Error analysis of image compression in the PCA algorithm.

Top m principal component images m	The portion of included ground information (%)	reduction ratio (Total bits of image / bits of compressed image)	ems (Total mean-squared error between the original image and the reconstructed image)
1	93.42	7.00	344.24
2	96.57	3.50	179.50
3	98.39	2.33	84.26
4	99.33	1.75	35.18
5	99.70	1.40	15.57
6	99.90	1.17	5.00
7	100	1	2.41×10^{-28}

 DOI: https://doi.org/10.26549/met.v7i1.12317

4. PCA Numerical Algorithm for Remote Sensing Image Noise Cancellation

In remote sensing imaging in the process of imaging and image transmission have the influence of noise, CCD (charge coupling device) noise is the most important in the process of imaging noise, filter the DC component of CCD noise and eliminate zero response offset and response inconsistency, can be considered the remaining CCD noise for the superposition of Gaussian noise and salt and pepper noise [4]. The pepper noise can be eliminated by median filtering, and the remaining Gaussian random noise will reduce the performance of almost all compression algorithms. The probability density function of the Gaussian random variable z is given by the following equation:

$$\text{The p (z)} = \frac{1}{\sqrt{2\pi}\sigma} e^{-(z-\mu)^2/2\sigma^2} \tag{13}$$

where z represents the gray value, the mean of z, is the standard deviation of z. Because Gaussian noise band and image band overlap, noise cannot be eliminated with traditional selective filter. As can be seen from Table 1, the amount of information contained in the remote sensing images after the main component transformation is gradually reduced, while the last three main component images contain very little ground object information. Since the Gaussian random noise components are uncorrelated (independent), the noise is highlighted when the information is reduced, so the transformation can separate the noise in the image.

The experimental environment in this section is the same as in Section 2, and the data are still derived from the same set of images in the Colorado River T M 1 to T M 7 band, but all include a mean =0, and the normalized variance^{2}Gaussian noise =0.09, the first 3 images see Figure 3(a), the seven images, the first 3 main component images see Figure 2(b), obviously, only the first main component image contains more ground information in the next two subpictures almost only noise, so only take the first main component image to reconstruct the original image sequence, obviously reconstructed image (Figure 2(c) listed 3) Gaussian noise is reduced. Using the mean-square signal-to-noise ratio $(SNR)_{ms}$). To measure the effect of noise elimination, the formula is:

$$SNR_{ms} = \frac{\sum_{i=1}^{7}\sum_{x=0}^{N-1}\sum_{y=0}^{M-1}\hat{f}(i,x,y)^2}{\sum_{i=1}^{7}\sum_{x=0}^{N-1}\sum_{y=0}^{M-1}[\hat{f}(i,x,y)-f(i,x,y)]^2} \tag{14}$$

$\hat{f}$ where f is the original image; it is the reconstructed image. The SNR of the original noisy image was the SNR_0=4.31, and the SNR of the reconstructed images is the SNR_1=30.07, together with the SNR_0. Compared with the 6.97 times higher, the PCA numerical algorithm has a strong ability to eliminate Gaussian noise.

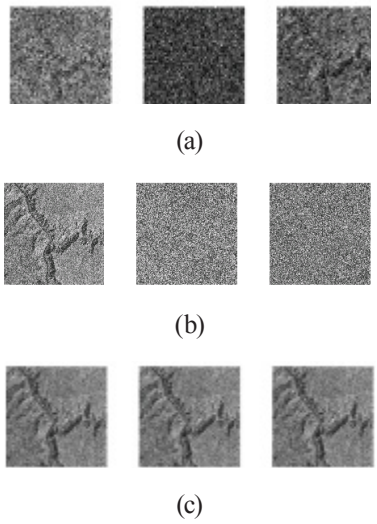

Figure 2. Remote sensing image noise cancellation by PCA numerical algorithm: (a) Multispectral images of the Colorado River with Gaussian noise; (b) Primary component image; (c) Denoised image only 3 pictures are listed.

5. The Numerical Algorithm of PCA Is a Remote Sensing Image Fusion

Remote sensing applications sometimes require both high spatial resolution and spectral resolution. However, imaging sensors of a single resource satellite are difficult to provide such data.

For example, the Landsat satellite can provide high spectral TM images with low resolution but low spatial resolution, while the Spot (Earth Observation Experimental System) satellite provides high spatial resolution panchromatic images with low spectral resolution. The key to solve this problem is the image fusion technology, which is to synthesize the scanning images of multiple sensors in the same area, and become a new image through the complementary information set, so as to achieve the effect of improving the spatial resolution while retaining the multispectral information [5].

PCA numerical algorithm image fusion experimental environment is the same as in section 2, the data comes from the spot TM image (Figure 3a) and the same area image (Figure 3b), Figure 3a, using PCA numerical algorithm, using the spot contrast linear stretch of the first main color image in Figure 3c, so it also maintains the color features of the color image high resolution, the color of the fusion image and the original image.

DOI: https://doi.org/10.26549/met.v7i1.12317

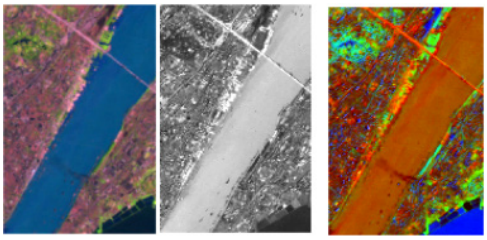

(a) (b) (c)

Figure 3. Remote sensing image fusion by PCA numerical algorithm: (a) TM multi-spectral visible light image; (b) Spot panchromatic image; (c) Fused image.

6. Conclusions

This paper presents the PCA numerical algorithm, available quickly in a computer, for compression, noise cancellation and fusion of remote sensing images, and verifies the effectiveness and accuracy of the algorithm with experiments.

References

[1] Wei, Y.Ch., Tang, G.A., Yang, X., et al., 2001. Remote sensing digital Image processing tutorial. Beijing: Science Press. pp. 1-30.

[2] Gonzalez, R.C., Woods, R.E., 2003. Digital image processing (Version 2). Beijing: Electronic Industry Press. pp. 550-560.

[3] Zhang, J., Lu, Y.H., Liu, Q.Y., 2006. Application of an improved embedded wavelet algorithm in remote sensing image compression. Microcomputer Information. (3-2), 79-81.

[4] Zhong, W.B., Ning, Sh.N., Jin, S.Z., et al., 2004. Remote sensing imaging noise analysis and the PCNN-based filtering method. Journal of Coal. (4), 418-421.

[5] Gao, Sh.Ch., 2006. VISUAL C + + practice and improvement: Digital image processing and engineering application. Beijing: China Railway Press. pp. 326-342.

 DOI: https://doi.org/10.26549/met.v7i1.12317